



Optics Letters

Efficient misalignment correction for annular LED arrays in intensity diffraction tomography

RUIZHI ZHU,^{1,2,†} WENJIE ZOU,^{1,2,†} RUNNAN ZHANG,^{1,2}  ZIHAO ZHOU,^{1,2}  JIASONG SUN,^{1,2} 
QIAN CHEN,²  NING ZHOU,^{1,2,3}  AND CHAO ZUO^{1,2,*} 

¹Smart Computational Imaging Laboratory (SCILab), Nanjing University of Science and Technology, Nanjing, Jiangsu 210094, China

²Jiangsu Key Laboratory of Spectral Imaging & Intelligent Sense, Nanjing, Jiangsu 210094, China

³zhouning@njust.edu.cn

[†]These authors contributed equally to this work.

*zuocho@njust.edu.cn

Received 22 January 2025; revised 21 March 2025; accepted 26 March 2025; posted 27 March 2025; published 23 April 2025

Intensity diffraction tomography (IDT) is a powerful label-free 3D microscopy technique capable of reconstructing the 3D refractive index (RI) of biological samples using angled programmable illumination and computational algorithms. Despite its potential for high spatiotemporal resolution imaging, its practical performance is highly sensitive to precise alignment between experimental setups and algorithmic models. In this Letter, we present an efficient misalignment correction method for annular LED arrays in IDT (mcIDT), incorporating an improved Fourier–Mellin transform (FMT) algorithm with enhanced noise resistance for wavelength and positional corrections. Furthermore, a global positional misalignment model is optimized using the least squares method, enabling robust correction even in the presence of significant misalignments. By integrating algorithmic “calibration” with physical position “correction,” mcIDT significantly enhances both the resolution and accuracy of 3D RI reconstruction. Experimental results on resolution targets and biological samples, such as HepG2 and C166 cells, demonstrate its superior resolution and robustness in label-free, high spatiotemporal resolution 3D volumetric imaging. The proposed mcIDT offers a flexible and efficient solution for label-free computational microscopy across diverse biological and industrial applications. © 2025 Optica Publishing Group. All rights, including for text and data mining (TDM), Artificial Intelligence (AI) training, and similar technologies, are reserved.

<https://doi.org/10.1364/OL.557164>

Computational microscopy, as an emerging technique, utilizes the inherent refractive index (RI) of transparent biological samples as a natural contrast mechanism. By combining the power of optical hardware and computational reconstruction, it reconstructs images from indirect measurements without the need for labeling and staining [1]. In recent years, through the analysis and study of the transfer function of the imaging system [2,3], the annular matched illumination scheme has demonstrated unique advantages in high spatiotemporal resolution imaging due to its optimized spectral response and data acquisition efficiency. The implementation of this technique is

relatively straightforward, involving the addition of a simple annular LED illumination module as the light source for commercial microscopes. It has been widely applied in quantitative phase imaging [4,5] and diffraction tomography [6,7]. Notably, these high-resolution imaging techniques demand extremely precise matching between experimental parameters and algorithmic models. Particularly in IDT, the 2D spectrum of the measured image needs to be projected onto a 3D Ewald spherical shell [8]. Even slight model deviations can lead to significant reconstruction artifacts and severely affect the accuracy of the reconstruction.

To improve reconstruction quality and align the inverse algorithm with the experimental setup, researchers have developed various LED self-calibration algorithms. The simulated annealing algorithm is a commonly used advanced self-calibration method. As a joint estimation solution, it can eliminate LED misalignment artifacts that typically manifest as low-frequency noise [9]. However, when the LED array is significantly misaligned, the simulated annealing algorithm may converge to a local optimum, as the number of random spectrum shifts for each LED element is limited [10]. If we increase the search range for each LED element during the simulated annealing (SA) process, it would slow down the runtime of the solver by an order of magnitude or more, making the computational time cost of reconstruction unacceptable. To further improve the speed of self-calibration algorithms, Eckert *et al.* proposed a method combining bright-field preprocessing and spectral iterative estimation, which has yielded good correction results in various scenarios [11]. Unfortunately, the aforementioned methods all rely on iterative steps in the reconstruction algorithm and typically require extensive user expertise. On the other hand, existing LED calibration methods only “calibrate” positions at the algorithmic level and do not involve physical displacement “correction.” Therefore, even if the position calibration is correct, the reconstruction artifacts and inaccurate RI caused by the misalignment between the light source and the optical axis still exist.

In this Letter, to overcome these challenges, we propose an efficient misalignment correction method for annular LED arrays in IDT (mcIDT). Leveraging the Fourier–Mellin transform (FMT) for the registration of image translation and scaling [12], we align the 2D spectrum of the actual captured image

with the aperture of the ideal model in the reconstruction algorithm. Specifically, we employ the normalized cross correlation (NCC) algorithm [13] in place of the phase correlation algorithm in the FMT workflow. This addresses the issue that the FMT algorithm requires a high overlap rate and good signal-to-noise ratio (SNR) between images, making it possible to correct the position and wavelength of the LED. Combined with a global positional misalignment model for annular LEDs, this approach further enhances the accuracy and robustness of the registration. Additionally, we emphasize the importance of mechanical displacement compensation for the LED array position. Both simulation and experimental results demonstrate that the mcIDT method achieves robust positioning and correction, significantly improving the accuracy of 3D RI reconstruction. We believe that the mcIDT method will provide a universal and efficient solution for the scientific research and industrialization of computational optical microscopes.

As shown in Fig. 1(a), under the annular matched illumination mode, the annular LED array is sequentially activated to illuminate the sample from various angles. As shown in Fig. 1(b), by performing a Fourier transform on the acquired intensity stack, the corresponding 2D spectrum can be obtained. Furthermore, based on the Fourier diffraction theorem, the scattering potential spectrum within the butterfly-shaped support domain is reconstructed in the 3D frequency space through deconvolution [6] or iterative IDT algorithms [14]. It is important to emphasize that the IDT algorithm, which relies on the inverse algorithm to retrieve sample parameters, requires an accurate modeling of the relationship between the measured data and the sample parameters. In actual experiments, misalignment of the annular LED array can cause a shift between the ideal aperture position (solid circle) and the actual aperture position (dashed circle), as shown in Fig. 1(c1). Additionally, since the diameter of the generalized aperture defined by the objective lens is determined by the wavenumber, different illumination wavelengths correspond to different aperture diameters. When the actual wavelength of the LED illumination is inconsistent with that set in the reconstruction algorithm, there will be an error in the aperture diameter, as shown in Fig. 1(d1). Furthermore, when the 2D Fourier spectrum is projected onto the 3D Ewald spherical shell, the offset of the 2D aperture can lead to a complete misalignment between the theoretical and actual positions of the 3D generalized aperture (Ewald spherical shell), resulting in significant reconstruction artifacts in the 3D RI results and severely affecting the reconstruction accuracy, as shown in Figs. 1(c2) and 1(d2). Therefore, correcting the misalignment is crucial for improving imaging accuracy.

The correction process for annular LED array misalignment is shown in Fig. 2. Firstly, a Fourier transform is performed on the captured intensity stack to convert the image from the spatial domain to the frequency domain. Due to the real-valued nature of the intensity image, which results in conjugate symmetry of the spectrum, we only need to consider one circle, as shown in Fig. 2(a). Based on the initial estimates of the experimental system parameters, we crop the spectrum along the tangent of the two circles. Furthermore, utilizing the registration capabilities of the FMT for image translation and scaling, we align the actual spectrum with the ideal pupil in the reconstruction algorithm, as shown in Fig. 2(b). However, the FMT method requires converting the image to log-polar coordinates to achieve scaling calibration (i.e., wavelength correction), which demands a high overlap rate and good SNR between images to collect sufficient

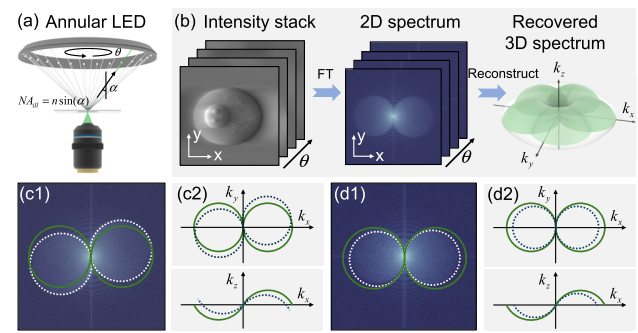


Fig. 1. Schematic diagram of intensity and its spectrum. (a) Annular LED array model. (b) Simulated image of cells and their Fourier spectra. (c) and (d) show the changes in the spectrum under the conditions of position deviation and wavelength deviation of the annular LED array.

features for correct image alignment in polar coordinates. Considering the presence of speckle noise in the spectrum, the phase correlation algorithm traditionally used in FMT is sensitive to noise and cannot operate stably, thereby reducing the accuracy of correction (noise resistance comparison analysis in Supplement 1, Section 1). Therefore, in this study, we replace the phase correlation algorithm with the robust NCC algorithm in the scaling correction workflow to achieve the preliminary correction of LED wavelength. The detailed process of the registration algorithm in Fig. 2(b) is provided in Supplement 1, Section 2. Further, combining the global positional misalignment model proposed in our previous work [6,10], we ensure that the corrected spatial distribution satisfies two physical prior constraints of the annular LED array: 1) the LED distribution follows a circular geometric shape and is equally spaced; 2) the LED is located on a horizontal plane perpendicular to the optical axis. As shown in Fig. 2(c), by solving the optimization problem of the global positional misalignment model using the least squares method, we can obtain three global offset factors for the annular LED array (rotation factor θ and offset factors Δx and Δy along the x axis and y axis), thereby reducing the impact of registration errors for individual LEDs and significantly improving the accuracy and robustness of registration. Finally, the wavelength is precisely corrected based on the calibrated LED coordinates. As shown in Fig. 2(d), the spectrum is rotated to the position where the circle center coordinate is $x = 0$ and then projected along the y -axis to obtain 1D data. After taking the second derivative, the diameter of the pupil can be obtained, and the precise corrected wavelength value can be calculated using the formula $f_{cut} = NA_{obj}/\lambda$. In addition, our algorithm has achieved a one-order-of-magnitude improvement in speed compared to the LED calibration algorithm we previously proposed [10] (Supplement 1, Table S1).

The annular matched illumination scheme optimizes spectral response and data acquisition efficiency, but it also demands higher coaxiality of the light source and the optical axis. As shown in Fig. 3(a1), under ideal matched illumination conditions, the two anti-symmetric pupils of the phase transfer function are tangent to each other, ensuring that phase information of the sample is fully transmitted to the intensity image. When the annular LED array shifts, the misalignment of the light source and the optical axis causes the illumination to move out of the ideal objective aperture position (green circle), allowing some dark-field information to enter the original image, as shown

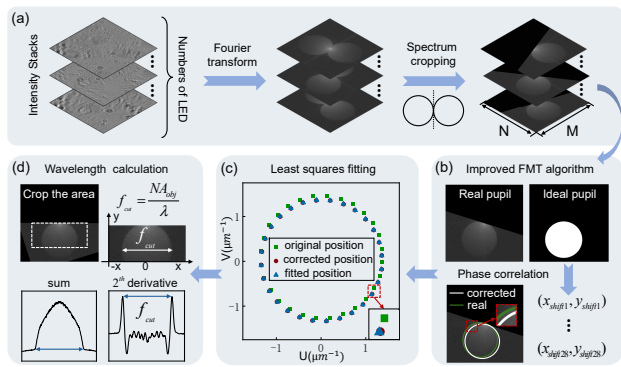


Fig. 2. Flow chart of the mcIDT algorithm. (a) Perform a Fourier transform on the intensity image to obtain the cropped spectrum. (b) Conduct an improved FMT algorithm on the cropped spectrum. (c) Fit the corrected spectral position using the least squares method. (d) Wavelength calculation.

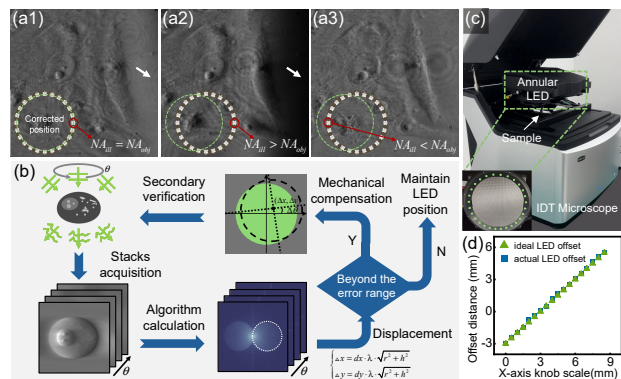


Fig. 3. Experimental setup and flow chart of the mcIDT method. (a1)–(a3) Images captured with the annular LED array at different positions. (b) Flow chart of the mcIDT method. (c) Experimental setup of the mcIDT. (d) Validation of algorithm effectiveness.

in Fig. 3(a2). Correspondingly, the illumination on the other side moves into the green circle, resulting in the illumination numerical aperture (NA) that is less than the objective NA, as shown in Fig. 3(a3). Under non-matched illumination conditions, the two pupils no longer perfectly overlap, and low-frequency phase components cannot be transmitted to the intensity image (Supplement 1, Section 4). When the misaligned original image is used for the IDT algorithm, even if the “calibration” of the position is adjusted at the algorithmic level to align the theoretical model with the experimental setup, the restored 3D RI values will still exhibit significant distortion. Therefore, the physical displacement “correction” of the annular LED array is an indispensable step. As shown in Fig. 3(b), the least squares algorithm is used to fit and output the required displacement distance, using the actual displacement corresponding to the frequency range of a single pixel point in the Fourier spectrum as the judgment condition to check whether the annular LED array meets the experimental requirements and then perform mechanical compensation and secondary calibration verification.

Based on the commercial inverted IDT microscope shown in Fig. 3(c) (Zircon-Pro, Zircon Optoelectronics (Suzhou) Co., Ltd.), we verified the correction capability of the algorithm. This microscope is equipped with a programmable annular LED

array with a radius of 97.51 mm (containing 28 surface-mounted LEDs with a wavelength of 517 nm and a full width at half maximum (FWHM) of 25 nm) as the light source (Supplement 1, Section 4). The module is installed on an x – y dual-axis displacement stage (LX20, Thorlabs) at a distance of 86 mm from the sample, capable of achieving a theoretical illumination NA of 0.75 for multi-angle illumination. Combined with a 40 \times /0.75 NA objective lens (UPLFLN40X, Olympus), it can realize matched illumination conditions. The original intensity stack was captured by a high-speed sCMOS camera (PCO.edge 5.5 CLHS). We moved the x –axis of the displacement stage linearly in 500 μ m steps, and after each movement, the algorithm was used to calibrate the displacement of the annular LED array from the optical axis, as shown in Fig. 3(d). The experimental results validated the accuracy and reliability of the algorithm.

To verify the effectiveness of the mcIDT method in enhancing the quality of 3D RI reconstruction, we conducted experimental measurements on unlabeled HepG2 cells. Figure 4(a) presents the reconstruction results of traditional IDT [15], algorithmically calibrated IDT (acIDT) that is based on the SA algorithm [10], and mcIDT methods when the annular LED array unexpectedly shifts and becomes misaligned. By magnifying the regions of interest (ROI) in Fig. 4(a), we compared the reconstruction effects of the three methods, as shown in Figs. 4(b) and 4(c). It can be observed that in different regions, the traditional IDT reconstruction algorithm without LED calibration results in significantly blurred 3D RI reconstruction and a substantial decrease in resolution. Although the acIDT reconstruction results can restore some image details, the issue of distortion in the reconstructed RI (as indicated by the white dashed circles in the figure) remains unavoidable. In contrast, the mcIDT method significantly improves the resolution and accuracy of 3D RI reconstruction. Figures 4(e)–4(g) display the profiles at different line positions in the magnified images. It is evident that the reconstruction results of traditional IDT and acIDT are not ideal. In contrast, the mcIDT method consistently demonstrates better results than traditional methods, with pixel values of details showing distinct peaks and valleys, revealing the unique morphology of filopodia. Additionally, we conducted the same experiments on a resolution target (Supplement 1, Section 3), further demonstrating the accuracy of the mcIDT method.

Finally, we applied the proposed mcIDT method to perform label-free time-lapse imaging of live C166 cells. In the experiment, the camera was optimized to a rectangular field of view composed of 1024 \times 1024 pixels and achieve a maximum acquisition rate of 212 Hz, in order to minimize artifacts caused by motion. Figure 5(a) shows the x – y slice and z -axis cross-sectional views reconstructed at the C166 cells at $t = 05:00$ in Visualization 1. In addition, we have also conducted microsphere experiments to verify the 3D RI result of the mcIDT method (Supplement 1, Section 4). Figures 5(b) and 5(c) display x – y slices at different axial depths of different regions at $t = 05:00$, showcasing high-resolution visualization of subcellular structures such as nucleoli, nuclear envelopes, lipid droplets, mitochondria, and dark vacuoles (indicated by white arrows). The dark vacuoles are vacuole-like structures that we observe in cells. The RI of dark vacuoles is lower than that of the cytoplasm, and they contain much fewer substances than the cytoplasm [16]. Figure 5(d) shows the 3D rendering image of Fig. 5(a). Figure 5(e) further illustrates key dynamics during the proliferation of C166 cells. The filopodia, acting as probing structures of the cell, trigger intercellular communication and cell polarization

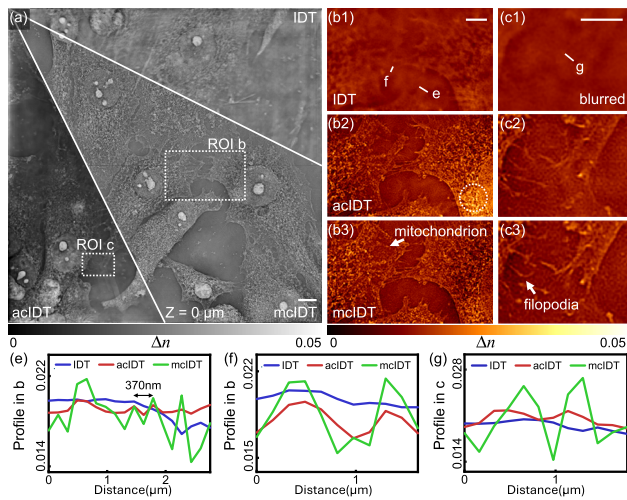


Fig. 4. Comparison of IDT results of HepG2 cells. (a) Comparison of 3D RI results under IDT, acIDT, and mcIDT methods when the annular LED array position is deviated. (b), (c) Enlarged images of the two boxed areas in (a). (e)–(g) RI profiles across subcellular structures. Scale bar, (a) 10 μm ; (b), (c) 5 μm .

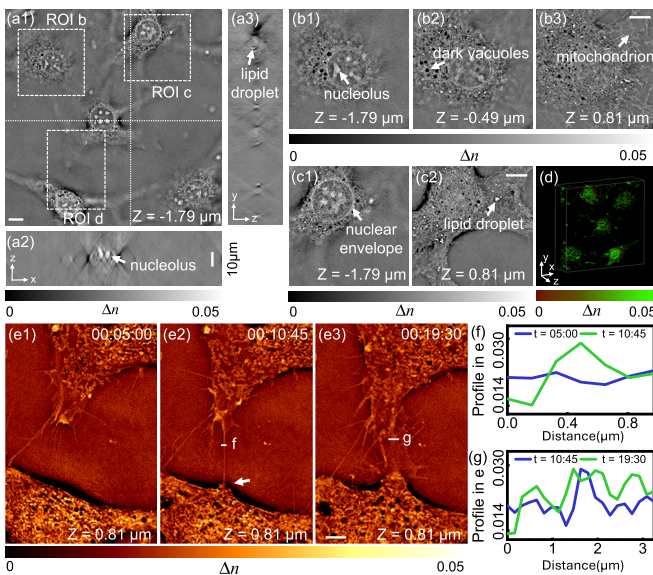


Fig. 5. 3D RI imaging of C166 cells under mcIDT method. (a) Large-field image of C166 cells. (b) and (c) are the magnified images in (a1). (d) is the 3D rendering of (a1). (e) is the long-term cell imaging of the selected region d in (a1). (f), (g) Comparison of line profiles of intracellular structures on different time. Scale bar, 10 μm .

upon contact with the cell wall. Figure 5(e3) shows the cell state of C166 cells at $t = 19:30$, where subcellular structures such as mitochondria and vacuoles appear in the connection area between two cells, indicating the initiation of material transport between cells. In Figs. 5(f)–5(g), line profiles across these submicron-level cellular structures demonstrate lateral resolution approaching the diffraction limit. The experimental results indicate that mcIDT has the capability for high spatiotemporal resolution imaging, which is crucial for the study of cell morphology and dynamics.

In conclusion, we have proposed mcIDT, an efficient misalignment correction method for annular LED arrays in spatiotemporal resolution IDT. Unlike the traditional techniques for position calibration, mcIDT firstly employs an improved FMT algorithm with enhanced noise resistance to perform initial correction of the wavelength and spatial position of the LED. Subsequently, it solves the optimization problem of the global misalignment model using the least squares method to achieve more accurate correction results. Furthermore, by combining mechanical displacement compensation of the annular LED array position and the annular matched illumination scheme, mcIDT can significantly enhance imaging quality while maintaining a volumetric rate of 7.5 Hz and a lateral resolution of 346 nm. It should be noted that for the IDT technique with partially coherent illumination [17], its transfer function is no longer a circle defined by the aperture size. Therefore, the mcIDT method is not universally applicable. In such cases, it is necessary to activate a single point of the partially coherent light source (when supported by hardware) and then perform calibration. Theoretical analysis and experimental results demonstrate that mcIDT is a universal and efficient self-calibration method, crucial for advancing the scientific research and industrial promotion of computational optical microscopes. It provides a powerful technical support for imaging in biomedicine and life sciences.

Funding. National Natural Science Foundation of China (62227818, 62361136588, 62305162); National Key Research and Development Program of China (2022YFA1205002, 2024YFE0101300); Biomedical Competition Foundation of Jiangsu Province (BE2022847); Key National Industrial Technology Cooperation Foundation of Jiangsu Province (BZ2022039); Fundamental Research Funds for the Central Universities (30920032101, 30923010206); Fundamental Research Funds for the Central Universities (2023102001); Open Research Fund of Jiangsu Key Laboratory of Spectral Imaging & Intelligent Sense (JSGP202105, JSGP202201, JSGPCXZNGZ202401).

Disclosures. The authors declare no conflicts of interest.

Data availability. Data underlying the results presented in this Letter are not publicly available at this time but may be obtained from the authors upon reasonable request.

Supplemental document. See Supplement 1 for supporting content.

REFERENCES

1. Y. Fan, J. Li, L. Lu, *et al.*, *PhotonIX* **2**, 19 (2021).
2. N. Zhou, J. Sun, R. Zhang, *et al.*, *ACS Photonics* **10**, 2461 (2023).
3. R. Zhang, N. Zhou, H. Tang, *et al.*, *Laser Photonics Rev.* **18**, 2300770 (2024).
4. C. Zuo, J. Sun, J. Li, *et al.*, *Sci. Rep.* **7**, 7654 (2017).
5. Y. Shu, J. Sun, J. Lyu, *et al.*, *PhotonIX* **3**, 24 (2022).
6. J. Li, A. Matlock, Y. Li, *et al.*, *Adv. Photonics* **1**, 066004 (2019).
7. N. Zhou, R. Zhang, W. Xu, *et al.*, *Laser Photonics Rev.* **18**, 2400387 (2024).
8. E. Wolf, *Opt. Commun.* **1**, 153 (1969).
9. L.-H. Yeh, J. Dong, J. Zhong, *et al.*, *Opt. Express* **23**, 33214 (2015).
10. J. Sun, Q. Chen, Y. Zhang, *et al.*, *Biomed. Opt. Express* **7**, 1336 (2016).
11. R. Eckert, Z. F. Phillips, and L. Waller, *Appl. Opt.* **57**, 5434 (2018).
12. Y. Dong, W. Jiao, T. Long, *et al.*, *Remote Sens.* **10**, 1719 (2018).
13. M. Guizar-Sicairos, S. T. Thurman, and J. R. Fienup, *Opt. Lett.* **33**, 156 (2008).
14. C. Zuo, J. Sun, J. Li, *et al.*, *Opt. Lasers Eng.* **128**, 106003 (2020).
15. R. Ling, W. Tahir, H.-Y. Lin, *et al.*, *Biomed. Opt. Express* **9**, 2130 (2018).
16. D. Dong, X. Huang, L. Li, *et al.*, *Light Sci. Appl.* **9**, 11 (2020).
17. J. Li, N. Zhou, Z. Bai, *et al.*, *Opt. Lasers Eng.* **143**, 106624 (2021).